Femtosecond laser-induced desorption of hydrogen molecules from Ru(0001): A systematic study based on machine-learned potentials

Steven Lindner,[†] Ivor Lončarić,[*,‡] Lovro Vrček,[¶,§] M. Alducin,[‖,⊥] J. I. Juaristi,[#,‖,⊥] and Peter Saalfrank[†]

[†]*Universität Potsdam, Institut für Chemie, Potsdam-Golm, Germany*

[‡]*Ruđer Bošković Institute, Zagreb, Croatia*

[¶]*Genome Institute of Singapore, A*STAR*

[§]*Faculty of Electrical Engineering and Computing, University of Zagreb, Croatia*

[‖]*Centro de Física de Materiales CFM/MPC (CSIC-UPV/EHU), Donostia-San Sebastián, Spain*

[⊥]*Donostia International Physics Center DIPC, Donostia-San Sebastián, Spain*

[#]*Departamento de Polímeros y Materiales Avanzados: Física, Química y Tecnología, Facultad de Químicas, Universidad del País Vasco (UPV/EHU), Donostia-San Sebastián, Spain*

E-mail: ivor.loncaric@gmail.com

Abstract

Femtosecond laser-induced dynamics of molecules on metal surfaces can be seamlessly simulated with all nuclear degrees of freedom using ab-initio molecular dynamics with electronic friction (AIMDEF) and stochastic forces which are a function of a time-dependent electronic temperature. This has recently been demonstrated for hot-electron mediated desorption of hydrogen molecules from a Ru(0001) surface covered with H and D atoms [Juaristi *et al.*, Phys. Rev. B **2017**, *95*, 125439]. Unfortunately, AIMDEF simulations come with a very large computational expense that severely limits statistics and propagation times. To keep ab-initio accuracy and allow for better statistical sampling, we have developed a neural network interatomic potential of hydrogen on the Ru(0001) surface based on data from ab-initio molecular dynamics simulations of recombinative desorption. Using this potential we simulated femtosecond laser-induced recombinative desorption using varying unit cells, coverages, laser fluences, and isotope ratios with reliable statistics. As a result, we can systematically study a wide range of these parameters and follow dynamics over longer times than hitherto possible, demonstrating that our methodology is a promising way to realistically simulate femtosecond laser-induced dynamics of molecules on metals. Moreover, we show that previously used cell sizes and propagation times were too small to obtain converged results.

1 Introduction

The use of femtosecond laser pulses to induce the dynamics of molecules on metal surfaces has a wide range of applications, including materials processing and time-resolved spectroscopy.[1,2] Intense femtosecond laser pulses can also be applied in surface photochemistry and photocatalysis, where increased reaction cross-sections, different reaction pathways, nonthermal product energy distributions, and even different products compared to those observed under thermal conditions, are observed.[1] Light pulses in the ultraviolet, visible, and near-infrared ranges are absorbed by the metal, leading to electronic excitations that are

then transferred to the lattice atoms through electron-phonon coupling. The interplay of direct electronic and indirect phononic energy transfer to the adsorbates triggers a range of photo-induced phenomena.[2]

One of the paradigmatic experimentally well-studied systems is femtosecond laser-induced recombinative desorption of H_2, D_2, and HD from Ru(0001) surfaces covered with atomic hydrogen or deuterium, see the detailed review in ref 3. Some of the conclusions of experimental studies are that the desorption process exhibits a significant isotope effect, with a higher probability of desorption for hydrogen (H_2) than deuterium (D_2). The desorption yield increases according to a power law with increasing fluence. The desorbing molecules have a velocity distribution that follows a Maxwell-Boltzmann distribution, but with a temperature that is much higher than expected from a purely thermal desorption mechanism. The translational temperature increases approximately linearly with fluence and is lower for D_2 than for H_2. The energy partitioning into translational, vibrational, and rotational energies of the desorbing species is unequal, and there is a preference for one type of rotation over the other. The ultrashort response time of the reaction, as observed in two-pulse correlation experiments, along with these other characteristics, suggests an electronic, non-thermal reaction mechanism. In addition, experiments using mixtures of the two isotopes found that the desorption of D_2 is facilitated by the presence of H at the surface, *i.e.*, a *dynamical promotion* effect was found,[4] while the desorption of H_2 is hindered by the presence of D.

Atomistic modeling of femtosecond laser-induced reactions on metal surfaces is complex, as many degrees of freedom and electronic excitations should be considered. Due to computational complexity, usually, either dimensionality or the explicit inclusion of excited states have to be sacrificed. Examples of such two models are quantum nonadiabatic approaches realized by the Monte Carlo wave packet method in the framework of open-system density matrix theory and the classical adiabatic approach that is realized with the help of frictional Langevin dynamics with stochastic forces.[5] In the quantum model only a few nuclear degrees of freedom can be considered and both ground and excited states, while the classical model

allows, in principle, all nuclear degrees of freedom, but only in the ground state. Being a paradigmatic model, laser-induced recombinative desorption of hydrogen from Ru(0001) was modeled in both fashions.[5–11] In passing we note that in order to treat multidimensional multi-surface dynamics for gas-surface problems, the independent-electron surface hopping (IESH) method has been introduced,[12] but so far not applied to surface photochemistry.

Due to the complex potential energy surfaces of molecules on surfaces, it is desirable to consider all nuclear degrees of freedom. As this can be practically achieved using frictional Langevin dynamics with stochastic forces, most of the recent studies use this approach.[7,10,13–16] Historically, due to the associated computational cost, still, only a few selected degrees of freedom were used. For the system of H/Ru(0001) Luntz *et al.*[10] used a three-dimensional model, and later Füchsel *et al.*[7] extended it to six dimensions (all degrees of freedom of two hydrogen atoms at a rigid surface). These studies used analytical potentials with parameters fitted to density functional theory (DFT) calculations. It is not easy to extend such analytical potentials to more than one molecule. Therefore, Juaristi *et al.*[17] used directly DFT forces in Langevin dynamics, the so-called ab-initio molecular dynamics with electronic friction (AIMDEF) method that was later used to study different photo-induced reactions.[18,19] This method allows studying more than two adsorbate atoms per unit cell with full dimensionality at the expense of orders of magnitude larger computational cost that severely limits statistical sampling. Specifically, in ref 17 the laser-induced desorption of hydrogen molecules from a (4×4) unit cell with 16 H (D) atoms was studied for a handful of selected H/D isotope ratios, at a single laser fluence and over a limited propagation time of 800 fs. In the present paper, we wish to go substantially beyond these limits in system size, H/D ratios, laser fluences, and propagation times to allow for a more systematic study. The key to do so is to make use of machine-learned potential energy surface.

In fact, an emerging tool in modeling dynamics is machine learning of interatomic potentials that can approach both the accuracy of the underlying ab-initio method and the speed of analytical potentials. For applications in simulations of femtosecond laser-induced

desorption, some of us have recently used the embedded atom neural network method[20] to create a machine learning potential of CO/Pd(111) that accurately reproduced the ab-initio results of ref 18 at a much lower computational cost.[21,22] Since the ab-initio data for the paradigmatic system of H/Ru(0001) already exist,[17] we have used these data to create a neural network potential. We then use this potential to simulate femtosecond laser-induced desorption with longer integration times, larger cell sizes, more coverages and isotope ratios as well as laser fluences than hitherto possible. This way, new and more detailed insight is gained into a non-trivial surface photoreaction.

2 Neural network potential for hydrogen / Ru(0001)

A potential energy surface is fitted with the neural network (NN) as implemented in the Atomistic Machine-learning Python Package (Amp).[23] The potential energy is computed as

$$E_{pot} = \sum_i E_i \tag{1}$$

from atomic energies E_i. As descriptors, we used Behler-Parrinello G^2 and G^4 symmetry functions,[24] given by

$$G_i^2 = \sum_{j \neq i} \mathrm{e}^{-\eta r_{ij}^2 / R_c^2} f_c(r_{ij}), \tag{2}$$

and

$$G_i^4 = 2^{1-\zeta} \sum_{j \neq i} \sum_{j \neq k} (1 + \lambda \cos\theta_{ijk})^\zeta \, \mathrm{e}^{-\eta\left(r_{ij}^2 + r_{ik}^2 + r_{jk}^2\right)/R_c^2} f_c\left(r_{ij}\right) f_c\left(r_{ik}\right) f_c\left(r_{jk}\right), \tag{3}$$

where

$$f_c\left(r\right) = \begin{cases} 0.5\left(1 + \cos\left(\pi \dfrac{r}{R_c}\right)\right) & \text{for } r \leq R_c, \\ 0 & \text{for } r > R_c. \end{cases} \tag{4}$$

Parameters η, ζ, and λ define the shape of symmetry functions, R_c is the cutoff radius, r_{ij} is the distance between atoms with index i and j, and θ_{ijk} is the angle between atoms i, j,

and k.

Training datasets are AIMDEF trajectories of ref 17. More details on the AIMDEF calculations can be found in that reference and in Sec. 3. Here it suffices to say that, all used trajectories were run with a modified version of the Vienna Simulation Package (VASP),[25,26] using DFT in the generalized gradient approximation to the exchange-correlation functional by Perdew-Becke-Ernzerhof (PBE)[27] and employing a plane wave basis. All trajectories used for training are for a three-layer slab model of a (4×4) Ru(0001) surface cell, fully covered with hydrogen, *i.e.*, trajectories start with 16 H atoms in 16 fcc sites of the surface – see Figure 2 below. In ref 17, all Ru atoms were kept fixed in their equilibrium position, a reasonable approximation due to the large mass mismatch between H/D and Ru atoms. We had access to more than 300 trajectories, each 8000 steps long with a time step of 0.1 fs. In total, that is over 2 400 000 DFT energies. For the initial training dataset, we sampled every 50th step of 250 trajectories. For the initial validation set, we sampled every 150th step, shifted for 20 steps compared to the training set. The training was performed on energies only using root-mean-square error (RMSE) as a loss function.

We have performed a hyperparameter search and selected the final model parameters. For the neural network architecture, the best-performing network had three hidden layers with 40-20-20 nodes. Selected descriptor parameters are listed in Table 1.

Table 1: Parameters of symmetry functions. A total of 20 symmetry functions are obtained from combinations of these parameters and permutations over two atom types for 2- and 3-body descriptors.

Descriptor	R_c (Å)	η	λ	ζ
G_i^2	4.5	0.05, 0.232, 1.077, 5.0		
G_i^4	4.5	0.005	1.0,-1.0	1.0, 4.0

Once we have determined hyperparameters and trained the neural network potential, we evaluated the complete dataset and found the configurations with the largest errors in forces. We expanded the training and validation sets to include the configurations with the largest errors in forces. Final training and validation sets consisted of 90 000 and 26 000

configurations and corresponding energies, respectively. The final potential was obtained by retraining on this new training set of energies and corresponding configurations. Figure 1 shows errors of the neural network potential compared to DFT data on a complete trajectory not included in the training set before and after retraining.

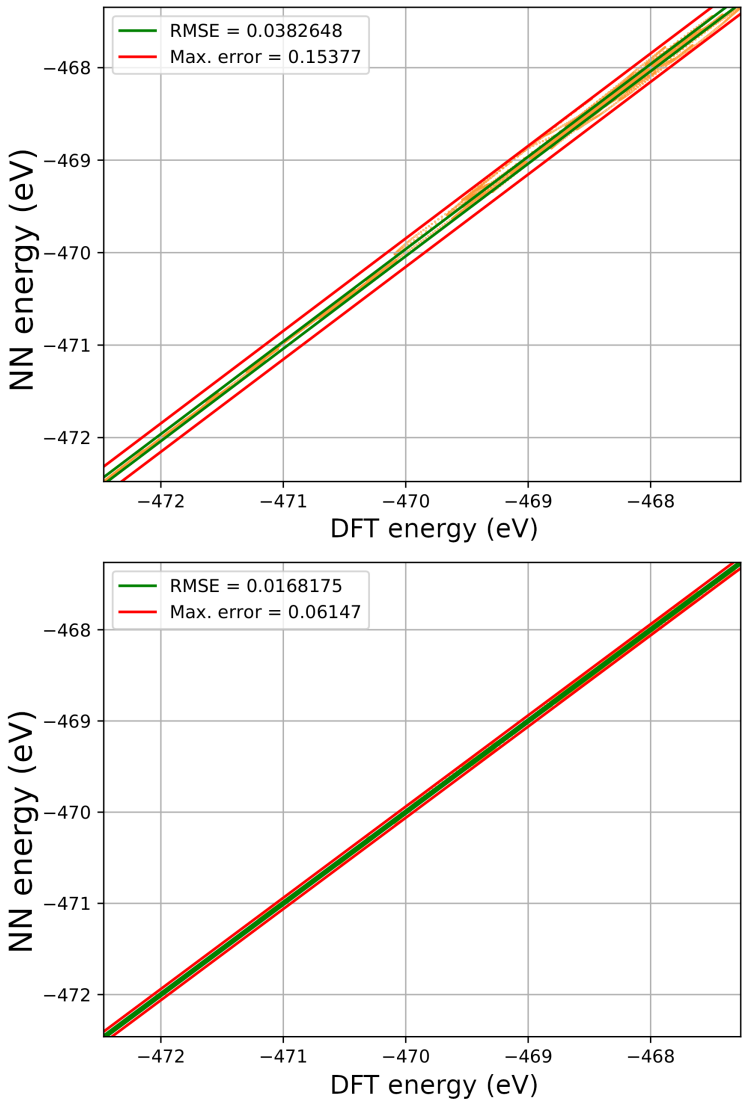

Figure 1: Comparison of DFT energies and neural network (NN) potential. Top panel: NN trained on the initial dataset. Bottom panel: NN trained on the final dataset. Red (green) lines are offset ± maximum error (RMSE) from perfect y=x line for which NN would predict exactly the same energy as DFT.

Both RMSE and maximum errors decreased more than twice. It can be seen that over the range of energies that span 5 eV (for the system of 16 H atoms), the RMSE of the refitted

potential is 0.017 eV with a maximum error of 0.061 eV. This error of ~ 1 meV per moving atom is similar to the error achieved for the CO/Pd(111) neural network potential.[21,22] Errors of the underlying DFT methodology are expected to be larger. This potential is used for all calculations presented below. Since these energies correspond to a temperature of adsorbates larger than 1000 K, this potential can be used also for other types of dynamics at lower temperatures. The potential is freely available, see ref 28.

One of the advantages of interpolated potential is that it is easy to investigate it in detail. Figure 2 shows a 2D cut of the potential as a function of the distance between two H atoms r and the distance from the surface Z (elbow plot). All other degrees of freedom and all other H and Ru atoms are fixed. Here, the two moving H atoms are initially in neighboring fcc sites of a (4×4) unit cell, fully covered with 16 H atoms. The classical barrier for desorption,

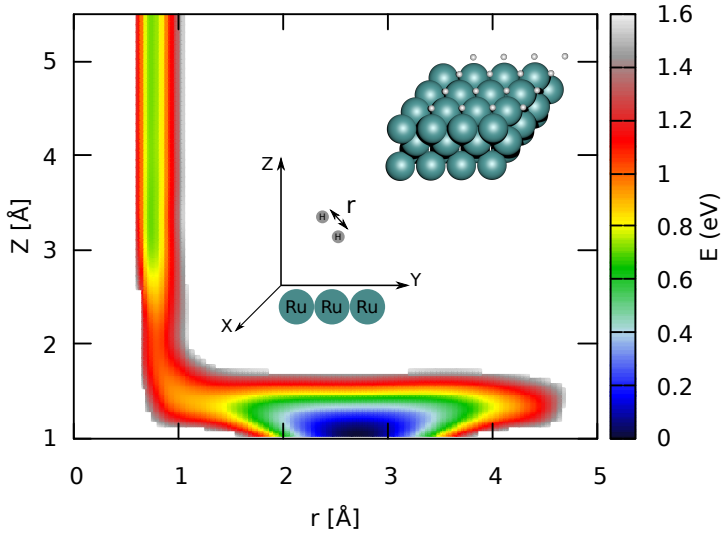

Figure 2: Potential energy surface as a function of distance between two H atoms, r, and distance from the surface, Z, of two H atoms parallel to the surface. All other degrees of freedom are fixed at the equilibrium positions of atoms adsorbed on the surface. Insets show the (4×4) unit cell and the Z and r coordinates.

counted from the potential minimum, is 1.01 eV in this elbow plot with $r = 0.79$ Å and $Z = 2.04$ Å, similar to previous studies.[5,10,17]

Nudged elastic band calculations[29,30] as implemented in the atomic simulation environment (ASE)[31] with default parameters were performed to find the minimum energy barrier

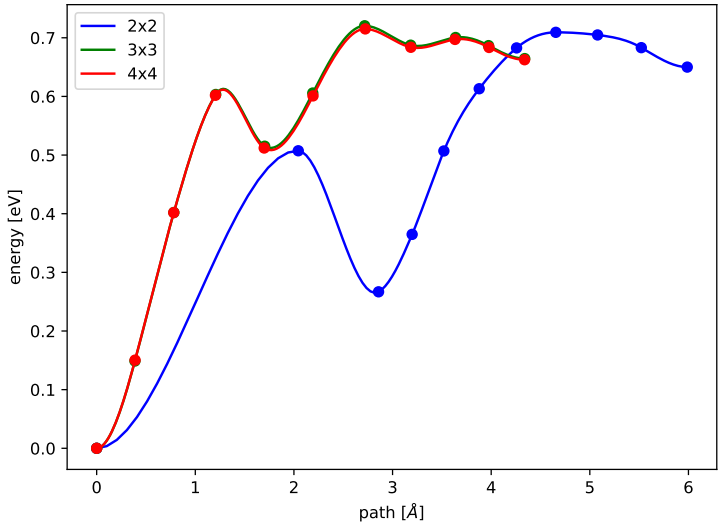

Figure 3: Potential energy as a function of the minimum energy path calculated with the nudged elastic band method for different unit cells at full (1 ML) coverage.

for recombinative desorption of two H atoms from neighbouring fcc sites in all dimensions (with a rigid surface, however). The minimum barrier is 0.72 eV for $r = 0.77$ Å and $Z = 2.39$ Å calculated for the (4×4) unit cell, *i.e.,* the barrier is substantially reduced when neighboring H atoms are allowed to rearrange along the reaction pathway. We have checked that the barrier and minimum energy path remains the same for (6×6) and (3×3) unit cells. As shown in Figure 3 there are also local minima in the minimum energy path at 2 Å for (3×3) and (4×4) unit cells and at 3 Å for the (2×2) unit cell. These minima correspond to situation when two H atoms become close to each other (r$\approx$ 0.8 Å), but still close to the surface (Z$\approx$ 2.7 Å).

In the case of a (2×2) unit cell, the barrier is the same, but the minimum energy path is significantly longer as shown in Figure 3. While for larger unit cells all H atoms but the two desorbing ones remain still close to their equilibrium fcc sites, in the case of (2×2) unit cell, the third H atom that is closest to the desorbing atoms moves from fcc to hcp site. This means that the configurational space leading to desorption is significantly different in the case of the (2×2) unit cell. Note that this is the cell that was used for all previous analytical potential constructions.[7,10] Below, we discuss the influence it has on the results of

laser-induced desorption simulations.

Even though the potential is trained on trajectories starting from full 1 ML (1×1) coverage, due to desorption, the potential is also trained on effectively lower coverages and can be used for such simulations. Experimentally, it is known that H adsorbed on Ru(0001) forms ordered structures for 1/3, 1/2, 3/4, and 1 ML.[32] In Table 2 we have calculated associative desorption energies, *i.e.*, minimal barriers for the desorption of a hydrogen molecule, for each of these structures in the (6×6) unit cell. It is seen from the table that the desorption energy rapidly increases as coverage decreases. As discussed below, and observed in experiments,[3] this also significantly decreases femtosecond laser-induced desorption for lower coverages.

Table 2: Associative desorption energy (the lowest desorption barrier) as a function of coverage, obtained for (6×6) unit cells.

Coverage	Structure[32]	Desorption energy (eV)
1/3 ML	p($\sqrt{3} \times \sqrt{3}$)	1.39
1/2 ML	p(2×1)	1.01
3/4 ML	(2×2)-3H	0.81
1 ML	(1×1)	0.72

3 Molecular dynamics with electronic friction

Molecular dynamics simulations are performed using frictional Langevin dynamics with stochastic forces as in earlier works[7,10,13–16]

$$m_i \frac{d^2\vec{r}_i}{dt^2} = -\vec{\nabla} V(\vec{r}_i) - \eta_{e,i}(\vec{r}_i)\frac{d\vec{r}_i}{dt} + \vec{R}_{e,i}[T_e(t), \eta_{e,i}(\vec{r}_i)]\,, \tag{5}$$

where V is the ground state potential energy surface, here modeled with the neural network potential, and $\eta_{e,i}$ is the electronic friction coefficient for atom i at position $\vec{r}_i$, calculated within the local density friction approximation (LDFA).[33] $\vec{R}_{e,i}$ is the corresponding random

fluctuation force obtained through the fluctuation-dissipation theorem with variance

$$\mathrm{Var}(\vec{R}_{e,i}[T_e(t), \eta_{e,i}(\vec{r}_i)]) = \frac{2k_B T_e(t)\eta_{e,i}(\vec{r}_i)}{\Delta t}\,, \tag{6}$$

where k_B and Δt are the Boltzmann constant and the time-integration step, respectively. $T_e(t)$ is the electronic temperature that is calculated within the two temperature model (2TM).[34] In the 2TM, we use the same material parameters for a Ru surface as in ref 17. Figure 4 shows solutions to the 2TM for Ru(0001) upon excitation with two different laser fluences, for laser pulses with Gaussian time-profile, full width at half maximum (FWHM) of 130 fs, and a wavelength of 800 nm. The initial temperature was set to 170 K.

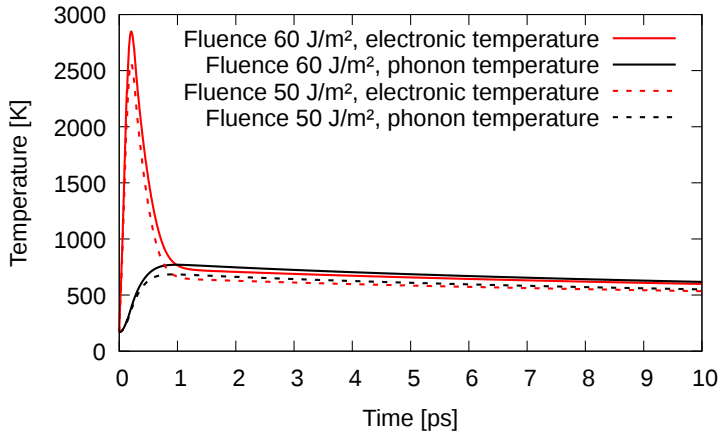

Figure 4: Electronic and phonon temperatures upon laser excitation of the Ru(0001) surface, calculated in the 2TM. Two different Gaussian pulses with FWHM=130 fs and wavelength=800 nm but different fluences have been used. Pulse maximum is at t=0.13 ps. The same material properties have been fed into the 2TM as in ref 17, and the same initial temperature (170 K).

Even though the 2TM provides both electronic and phonon temperatures, $T_e(t)$ and $T_p(t)$, here we use only the electronic temperature. Ruthenium atoms are fixed as in ref 17. Note that, if necessary, the methodology can be extended to include phonon temperature, as shown for the CO/Pd(111) system,[21,22] for example.

We implemented eq. (5) in ASE[31] that we use for all dynamics calculations. In the LDFA, η_e depends only on the electron density of bare Ru(0001) at the position of the adsorbate,

$\vec{r}_i$. We use the same DFT electron density of the bare Ru(0001) surface as in ref 17. The integration time step in all dynamics simulations is 0.1 fs to ensure stable integration.

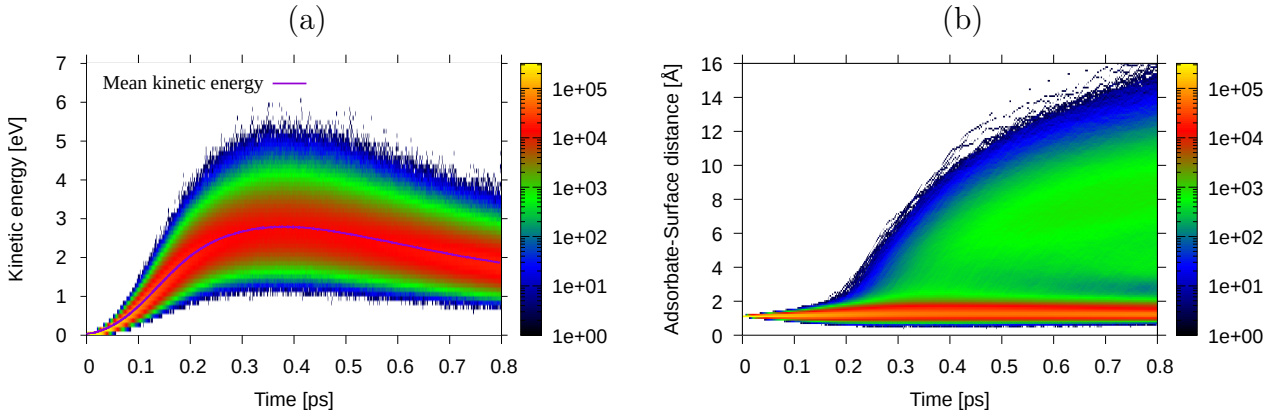

Figure 5: Histograms of the kinetic energy (a) and H-surface distance (b) over 20 000 trajectories with laser fluence of 60 J/m^2.

Since the neural network potential is by orders of magnitude faster than DFT, it is easy to run many more trajectories than in ab-initio molecular dynamics. In Figure 5(a) we follow energies and positions of adsorbates over 20 000 trajectories which should be compared to only 40 trajectories in the AIMDEF-DFT study[17] per one experimental condition. In the figure, we use the same (4×4) unit cell covered by H atoms and the same laser pulse of 60 J/m^2 as in ref 17 so that our results can be directly compared. Later, different fluences and cell sizes will also be considered in the present work.

According to Figure 5(a), the kinetic energy of adsorbates rises rapidly upon laser pulse excitation, reaching its maximum at about 0.37 ps after the pulse start. The maximum average kinetic energy of 2.8 eV or 0.175 eV per each of the 16 adsorbates is in agreement with Figure 5 of ref 17, confirming that our potential gives rise to similar dynamics and DFT forces. However, our statistics with a very smooth average line is superior to the noisy line of ref 17. From the color bar of Figure 5(a) it is also possible to see how probable is each kinetic energy, showing that kinetic energy in rare cases can be twice as large as the average kinetic energy at any given time.

Figure 5(b) shows the probability of distance from the surface for each H atom as a

function of time. It can be seen that desorption events start as early as 0.2 ps after laser excitation, while the highest number of atoms in the desorbing channel takes place when the kinetic energy is the highest, between 0.3 and 0.4 ps after pulse excitation.

Next, we have also studied dynamics when deuterium (D) is mixed with hydrogen on the surface. Figure 6 shows the desorption yield (Y) as a function of time for an equal ratio of H

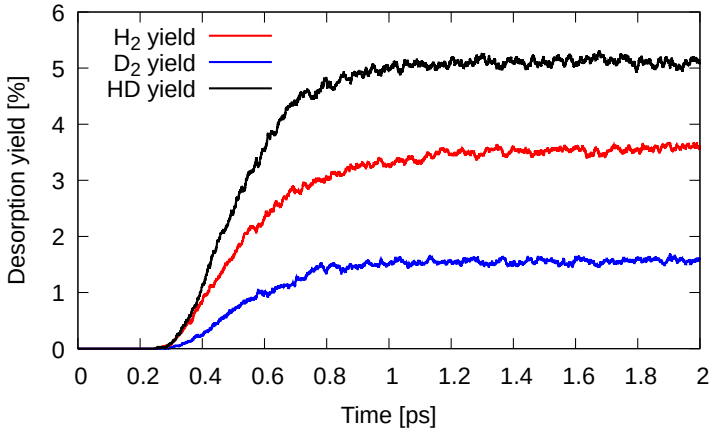

Figure 6: Desorption yield of H_2, HD, and D_2 for randomly placed H_8D_8 isotope mixture as a function of integration time for the laser fluence of 50 J/m^2.

and D randomly placed on the same (4×4) surface unit cell (H_8D_8), now for a fluence of 50 J/m^2. First, it can be seen that the integration time of 800 fs used in ref 17 does not result in completely converged results. The integration time in that study was constrained due to the associated large computational cost. Due to the speed of our potential evaluation, all our results are calculated with an integration time of 2 ps for which yields are well converged.

Figure 7 shows desorption yields for different isotope mixtures on the surface as symbols. Each yield is calculated over 2000 trajectories, each trajectory is initiated with a randomly placed H and D in each adsorption site using the same (4×4) unit cell. The fluence was 50 J/m^2 in all cases. Desorption of H_2 is more likely and faster compared to HD and D_2 as also observed in experiments.[35] The isotope ratio, defined as $Y(H_2)/Y(D_2)$ is experimentally found to be $\sim$20 for a fluence of 50 J/m^2 while we obtain $\sim$1.6. Experimentally,[4] a so-called dynamical promotion / suppression effect was found, where desorption of D_2 was larger and desorption of H_2 was smaller than expected from second order rate equations, in which a

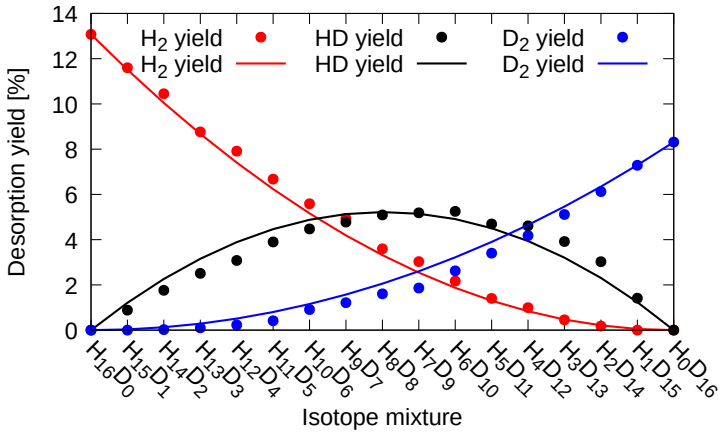

Figure 7: Desorption yield of H_2, HD, and D_2 for different isotope mixtures for the laser fluence of 50 J/m^2. Symbols are from the Langevin trajectories, solid lines from idealized second order rate models (see text and ref 17).

desorbing molecule is assumed to be unaffected by neighboring adsorbates (see ref 17 for details). The results of the second order rate equations are shown in Figure 7 as solid lines. It is seen that the deviation of the Langevin molecular dynamics simulations from the rate model are small, but a bit more H_2 desorption and a bit less of D_2 desorption is seen in the former. These differences to experiments are discussed below after all comparisons to experiments are made.

One of the hallmarks of short and intense laser-pulse-induced reactions at surfaces is that their yield depends superlinearly on fluence. In Figure 8 we show the desorption yield of H_2 from a fully covered (4×4) cell, as a function of fluence for fluences in the range of 10-60 J/m^2. Note that the training data is for fluence of 60 J/m^2, so using larger fluences would result in an extrapolation regime for our neural network potential. We observe a superlinear behavior, with an exponent of about 1.8. One can also observe the onset of a saturation regime for fluences larger than 40 J/m^2. Before saturation, the exponent is around 1.9. Fitting experimental yields before saturation results in a slightly larger exponent of 2.8, and saturation is reached only at around 100 J/m^2.[35]

Further, in ref 35, no desorption for coverages lower than 0.5 ML was found. In Figure 9 we show, for a (4×4) cell, desorption yields for H_2 and D_2 as a function of coverage with either

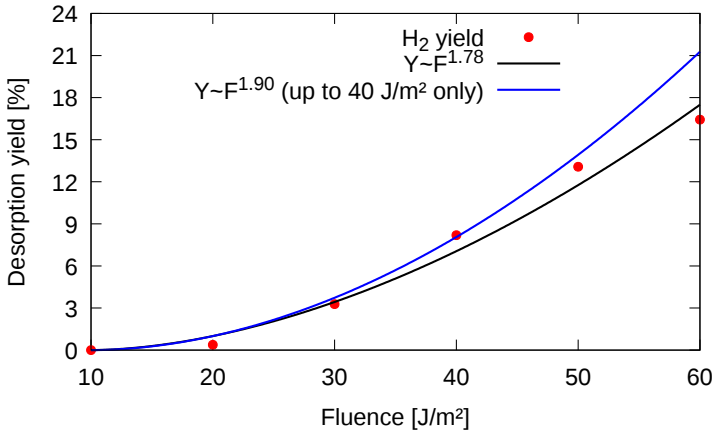

Figure 8: H_2 desorption yield as a function of laser fluence, for a fully H-covered (4×4) cell. Black line is fitted to all points, while blue line is fitted to fluence up to 40 J/m^2.

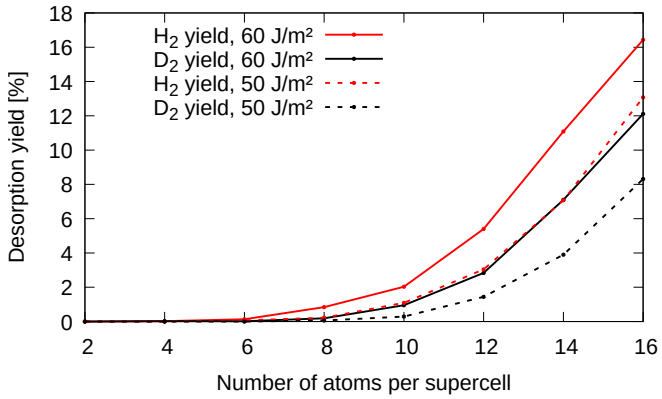

Figure 9: Yield as a function of coverage for (4×4) unit cell with 16 adsorption sites, for H_2 and D_2 and two different fluences.

H or D atoms. Coverages between 1/8 (2 adsorbate atoms per supercell) and 1 (16 atoms per supercell) are considered. We again obtain qualitative agreement with experiments, but desorption is possible even for coverages of about 0.375 ML (or 6 adsorbate atoms per (4×4) cell). Note that previous theoretical studies did not simulate coverage dependence as previous analytical potentials by construction could not simulate it, and in DFT-based dynamics, these simulations are expensive, especially when low yields are expected. In ref 35 the authors proposed that the results can be explained by the coverage dependence of the binding energy and/or the electronic friction coefficient. In our methodology, the electronic friction coefficient does not depend on the coverage, but as can be seen in Table 2, the

desorption barrier indeed depends strongly on coverage. Since the barrier for desorption is much higher for low coverages, desorption yields are much lower. Again, at a given coverage, H_2 desorbs easier than D_2, and yields are larger for larger laser fluences.

In summary, our simulations, as well as simulations in ref 17 show qualitative, but not fully quantitative agreement with experiments. As already explained in ref 17, differences can largely be attributed to too low binding / activation energy predicted by PBE[27] DFT. In fact, in simpler, low-dimensional or effective models, the energy barrier to desorption that agreed well with various experimental data was in the range of 1.042 eV in ref 8 to 1.35 eV in ref 35, compared with our lowest barrier of 0.72 eV. Note that low barriers lead to larger yields, hence to lower isotope ratios compared to experiment, (slightly) too low superlinearity and, apparently lack of dynamical promotion / suppression effects.

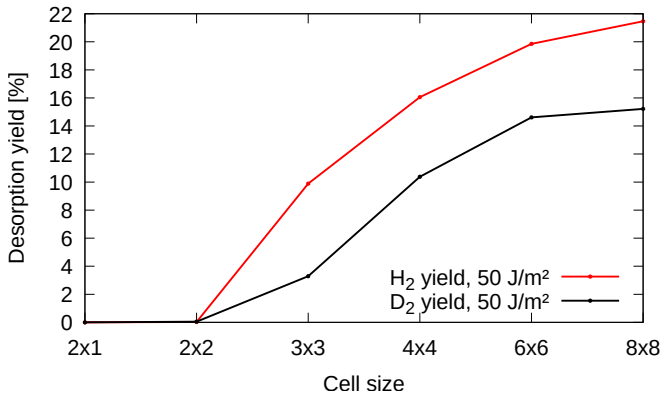

Figure 10: H_2 and D_2 desorption yields as a function of cell size, for 1ML adsorbates (coverage=1), and a fluence of 50 J/m^2.

We have also performed molecular dynamics simulations for different cell sizes, from (2×1) up to (8×8), always at full coverage. Results are shown in Figure 10. Clearly, simulations using smaller unit cells severely underestimate desorption yields. One can rationalize this result with a reduced configurational space, leading to desorption, in smaller unit cells as shown in Figure 3. This shows that better agreement of theoretical studies with experimental isotope ratios and desorption yields prior to ref 17, *e.g.* in ref 7, can be due to the fact that in ref 7, a single moving H_2/D_2 in a (2×2) cell was considered and the somewhat too

low desorption energy (1.042 eV compared to the effective barrier of 1.35 eV in ref 35) was compensated with a reduced configurational space. Note that even the AIMDEF methodology using already, for DFT, very large (4×4) unit cells underestimates yields as much as 50%. Only with very large unit cells such as (6×6) and (8×8) we obtain convergence in yields. Therefore, true first principles agreement with experiment should be achievable only with the methodology presented in this manuscript, but trained on DFT data calculated with more accurate exchange-correlation functional. Note also that in this particular case DFT data corresponds to only 3-layer slab that does not provide fully converged results, and all Ru atoms were fixed neglecting energy exchange with the surface.

4. Conclusion and Outlook

We have developed a neural network interatomic potential for H atoms interacting with a Ru(0001) surface. The potential was trained on the data from ab-initio molecular dynamics simulations of laser-induced desorption. As during these simulations, high adsorbate temperatures in excess of 1000 K are achieved, the potential is expected to be useful also for other studies involving lower temperatures.

Using this potential, we have simulated laser-induced recombinative desorption of H and D that is experimentally well studied. We compared our molecular dynamics simulations to previous ab-initio dynamics on which the potential was trained and to experimental data. Our machine-learned potential agrees well with the one from ab-initio dynamics. Results of both are in good qualitative, but not fully quantitative agreement with experiments. Namely, the PBE-based dynamics and the corresponding NN potential predicts somewhat too small desorption barriers, and as a consequence, too large desorption yields, too small isotope effect, too low saturation fluence for superlinear dependence on fluence, and, also, too small effects of a dynamic environment.

Due to the complex potential energy surface, a requirement for large unit cells, long

propagation times, and many trajectories needed for reliable statistics, we suggest that state-of-the-art simulations of short laser pulse-induced dynamics should follow our methodology. The first step is the construction of machine learning interatomic potential that should be trained on the configurations that sample well the configurational space explored in dynamics. The second step is to converge the integration time, cell size, and the number of needed trajectories. Once this is set, the final step is then to run Langevin molecular dynamics simulations with electronic friction and stochastic forces that depend on the two-temperature model.

Acknowledgement

This work has been supported in part by Croatian Science Foundation under the project UIP-2020–02-5675. J.I.J., and M.A. acknowledge financial support by the Gobierno Vasco-UPV/EHU [Project No. IT1569-22] and by the Spanish MCIN/AEI/10.13039/501100011033 [Grant No. PID2019-107396GB-I00]. P.S. acknowledges support by the Deutsche Forschungsgemeinschaft (DFG), through project Sa 547-18.

References

(1) Frischkorn, C.; Wolf, M. Femtochemistry at Metal Surfaces:Nonadiabatic Reaction Dynamics. *Chem. Rev.* **2006**, *106*, 4207–4233.

(2) Saalfrank, P. Quantum Dynamical Approach to Ultrafast Molecular Desorption from Surfaces. *Chem. Rev.* **2006**, *106*, 4116–4159, PMID: 17031982.

(3) Frischkorn, C. Ultrafast reaction dynamics of the associative hydrogen desorption from Ru(001). *Journal of Physics: Condensed Matter* **2008**, *20*, 313002.

(4) Denzler, D. N.; Frischkorn, C.; Hess, C.; Wolf, M.; Ertl, G. Electronic Excitation and Dynamic Promotion of a Surface Reaction. *Physical Review Letters* **2003**, *91*.

(5) Vazhappilly, T.; Klamroth, T.; Saalfrank, P.; Hernandez, R. Femtosecond-laser desorption of H_2 (D_2) from Ru (0001): Quantum and classical approaches. *The Journal of Physical Chemistry C* **2009**, *113*, 7790–7801.

(6) Füchsel, G.; Klamroth, T.; Tremblay, J. C.; Saalfrank, P. Stochastic approach to laser-induced ultrafast dynamics: the desorption of H_2/D_2 from Ru(0001). *Phys. Chem. Chem. Phys.* **2010**, *12*, 14082–14094.

(7) Füchsel, G.; Klamroth, T.; Monturet, S.; Saalfrank, P. Dissipative dynamics within the electronic friction approach: The femtosecond laser desorption of H_2/D_2 from Ru(0001). *Physical Chemistry Chemical Physics* **2011**, *13*, 8659–8670.

(8) Füchsel, G.; Tremblay, J. C.; Klamroth, T.; Saalfrank, P.; Frischkorn, C. Concept of a single temperature for highly nonequilibrium laser-induced hydrogen desorption from a ruthenium surface. *Physical Review Letters* **2012**, *109*, 098303.

(9) Füchsel, G.; Tremblay, J. C.; Klamroth, T.; Saalfrank, P. Quantum Dynamical Simulations of the Femtosecond-Laser-Induced Ultrafast Desorption of H_2 and D_2 from Ru(0001). *ChemPhysChem* **2013**, *14*, 1471–1478.

(10) Luntz, A.; Persson, M.; Wagner, S.; Frischkorn, C.; Wolf, M. Femtosecond laser induced associative desorption of H 2 from Ru (0001): Comparison of "first principles" theory with experiment. *The Journal of chemical physics* **2006**, *124*, 244702.

(11) Vazhappilly, T.; Beyvers, S.; Klamroth, T.; Luppi, M.; Saalfrank, P. Vibrationally enhanced associative photodesorption of molecular hydrogen from Ru(0001). *Chemical Physics* **2007**, *338*, 299–311.

(12) Shenvi, N.; Roy, S.; Tully, J. C. Nonadiabatic dynamics at metal surfaces: Independent-electron surface hopping. *The Journal of Chemical Physics* **2009**, *130*, 174107.

(13) Scholz, R.; Floß, G.; Saalfrank, P.; Füchsel, G.; Lončarić, I.; Juaristi, J. I. Femtosecond-laser induced dynamics of CO on Ru(0001): Deep insights from a hot-electron friction model including surface motion. *Phys. Rev. B* **2016**, *94*, 165447.

(14) Lončarić, I.; Alducin, M.; Saalfrank, P.; Juaristi, J. I. Femtosecond-laser-driven molecular dynamics on surfaces: Photodesorption of molecular oxygen from Ag(110). *Phys. Rev. B* **2016**, *93*, 014301.

(15) Loncaric, I.; Alducin, M.; Saalfrank, P.; Juaristi, J. I. Femtosecond laser pulse induced desorption: A molecular dynamics simulation. *Nuclear Instruments and Methods in Physics Research Section B: Beam Interactions with Materials and Atoms* **2016**, *382*, 114–118.

(16) Scholz, R.; Lindner, S.; Lončarić, I.; Tremblay, J. C.; Juaristi, J. I.; Alducin, M.; Saalfrank, P. Vibrational response and motion of carbon monoxide on Cu(100) driven by femtosecond laser pulses: Molecular dynamics with electronic friction. *Phys. Rev. B* **2019**, *100*, 245431.

(17) Juaristi, J. I.; Alducin, M.; Saalfrank, P. Femtosecond laser induced desorption of H_2, D_2, and HD from Ru(0001): Dynamical promotion and suppression studied with ab initio molecular dynamics with electronic friction. *Phys. Rev. B* **2017**, *95*, 125439.

(18) Alducin, M.; Camillone, N.; Hong, S.-Y.; Juaristi, J. I. n. Electrons and Phonons Cooperate in the Laser-Induced Desorption of CO from Pd(111). *Phys. Rev. Lett.* **2019**, *123*, 246802.

(19) Tetenoire, A.; Ehlert, C.; Juaristi, J. I.; Saalfrank, P.; Alducin, M. Why Ultrafast Photoinduced CO Desorption Dominates over Oxidation on Ru(0001). *J. Phys. Chem. Lett.* **2022**, *13*, 8516–8521.

(20) Zhang, Y.; Hu, C.; Jiang, B. Embedded Atom Neural Network Potentials: Efficient and

Accurate Machine Learning with a Physically Inspired Representation. *J. Phys. Chem. Lett.* **2019**, *10*, 4962–4967.

(21) Serrano Jiménez, A.; Sánchez Muzas, A. P.; Zhang, Y.; Ovčar, J.; Jiang, B.; Lončarić, I.; Juaristi, J. I.; Alducin, M. Photoinduced Desorption Dynamics of CO from Pd(111): A Neural Network Approach. *Journal of Chemical Theory and Computation* **2021**, *17*, 4648–4659.

(22) Muzas, A.; Serrano Jiménez, A.; Ovčar, J.; Lončarić, I.; Alducin, M.; Juaristi, J. I. Absence of isotope effects in the photo-induced desorption of CO from saturated Pd(111) at high laser fluence. *Chemical Physics* **2022**, *558*, 111518.

(23) Khorshidi, A.; Peterson, A. A. Amp: A modular approach to machine learning in atomistic simulations. *Computer Physics Communications* **2016**, *207*, 310–324.

(24) Behler, J. Atom-centered symmetry functions for constructing high-dimensional neural network potentials. *The Journal of Chemical Physics* **2011**, *134*, 074106.

(25) Kresse, G.; Furthmüller, J. Efficient iterative schemes for ab initio total-energy calculations using a plane-wave basis set. *Physical Review B* **1996**, *54*, 11169.

(26) Kresse, G.; Joubert, D. From ultrasoft pseudopotentials to the projector augmented-wave method. *Physical Review B* **1999**, *59*, 1758.

(27) Perdew, J. P.; Burke, K.; Ernzerhof, M. *Physical Review Letters* **1998**, *80*, 891–891.

(28) Lindner, S.; Lončarić, I.; Vrček, L.; Alducin, M.; Juaristi, J.; Saalfrank, P. Neural network potential for H/Ru(0001). 2023; `https://doi.org/10.5281/zenodo.7896157`.

(29) Henkelman, G.; Jónsson, H. Improved tangent estimate in the nudged elastic band method for finding minimum energy paths and saddle points. *The Journal of Chemical Physics* **2000**, *113*, 9978–9985.

(30) Henkelman, G.; Uberuaga, B. P.; Jónsson, H. A climbing image nudged elastic band method for finding saddle points and minimum energy paths. *The Journal of Chemical Physics* **2000**, *113*, 9901–9904.

(31) Larsen, A. H.; Mortensen, J. J.; Blomqvist, J.; Castelli, I. E.; Christensen, R.; Dułak, M.; Friis, J.; Groves, M. N.; Hammer, B.; Hargus, C. et al. The atomic simulation environment—a Python library for working with atoms. *Journal of Physics: Condensed Matter* **2017**, *29*, 273002.

(32) Tatarkhanov, M.; Rose, F.; Fomin, E.; Ogletree, D. F.; Salmeron, M. Hydrogen adsorption on Ru(001) studied by scanning tunneling microscopy. *Surface Science* **2008**, *602*, 487–492.

(33) Juaristi, J. I.; Alducin, M.; Muiño, R. D.; Busnengo, H. F.; Salin, A. Role of Electron-Hole Pair Excitations in the Dissociative Adsorption of Diatomic Molecules on Metal Surfaces. *Physical Review Letters* **2008**, *100*.

(34) Anisimov, S. I.; Kapeliovich, B. L.; Perel'man, T. L. Electron emission from metal surfaces exposed to ultrashort laser pulses. *JETP* **1973**, *39*, 375.

(35) Denzler, D. N.; Frischkorn, C.; Wolf, M.; Ertl, G. Surface Femtochemistry: Associative Desorption of Hydrogen from Ru(001) Induced by Electronic Excitations. *The Journal of Physical Chemistry B* **2004**, *108*, 14503–14510.